Construction and Building Materials 501 (2025) 144385

Contents lists available at ScienceDirect

Construction and Building Materials

journal homepage: www.elsevier.com/locate/conbuildmat

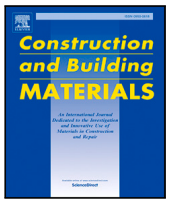

Temperature effect on the tensile constitutive parameters of fiber reinforced concrete

Federico Ponsi [a], Elisa Bassoli [a,*], Claudio Mazzotti [b], Nicola Buratti [b], Loris Vincenzi [a]

[a] University of Modena and Reggio Emilia, Department of Engineering "Enzo Ferrari" (DIEF), Modena, Italy
[b] University of Bologna, Department of Civil, Chemical, Environmental and Materials Engineering (DICAM), Bologna, Italy

ARTICLE INFO

Keywords:
Macro-synthetic fiber reinforced concrete
Temperature effect
Cohesive crack model
Inverse analysis
Prediction model

ABSTRACT

This paper focuses on the effect of moderate temperature variations on the flexural behavior of polypropylene macro-synthetic fiber reinforced concrete. A comprehensive study has been carried out to investigate the influence of temperature on the tensile constitutive parameters. The study is based on the results of an experimental campaign consisting of compression tests and three point bending tests conducted on specimens cured at different temperatures, ranging from -30 °C to 60 °C. The core of the research is the calibration of the relationship between the constitutive parameters for polypropylene macro-synthetic fiber reinforced concrete and temperature values. A hybrid regression model is developed to describe the relationship and the most adequate regression model is selected among several alternatives according to the Akaike Information Criterion. It involves a bi-linear relationship between each one of the constitutive parameters and temperature, with a common transition temperature for the parameters mostly related to the post-cracking behavior. This model proves to be well suited to describe the temperature effect for different polypropylene macro-synthetic fiber reinforced concretes and it provides valuable insights for structural applications. The paper also presents the procedure for the estimation of the hybrid regression model, which can be adopted for modeling the temperature effect on fiber reinforced concretes constituted by materials of different properties.

1. Introduction

Macro-synthetic fiber reinforced concrete with polypropylene fibers (PP-MSFRC) is undergoing a considerable diffusion for the improved mechanical properties, energy absorption capacity and crack bridging ability compared to plain concrete [1,2]. The different structural applications regarding PP-MSFRC imply an exposition to varying environmental conditions [3,4] and this aspect can affect its behavior. In particular, mechanical properties of PP-MSFRC like compressive strength, tensile strength, modulus of elasticity, and flexural tensile strength are sensitive to temperature change, thus affecting the final structural performance. This work is not interested in the behavior at very high temperatures due to fire events, already studied by many authors [5–7], but rather to the influence of moderate temperature variations in service conditions.

In the past years, specific experimental campaigns have been carried out in this regard. Buratti and Mazzotti [8] investigated for the first time the effects of moderate temperature variations on the short and long term behavior of cracked MSFRC. For the former, three-point bending tests (TPBTs) were carried out at 20 °C and 40 °C on four different types of MSFRC. Two of these were sensitive to temperature variations, while for the remaining two no remarkable effects were observed. For the long term test, temperature ranged between 20 °C and 50 °C. These variations can have significant effects and in some cases trigger creep failure. Caballero-Jorna et al. [9] performed an experimental investigation on fiber reinforced concrete containing steel or macro-synthetic fibers. Specimens were conserved at temperatures of 5, 20, 35 and 50 °C and tested in TPBTs. Results revealed that for both fiber types the temperature effects are more noticeable for larger Crack Mouth Opening Displacement (CMOD) compared to a small CMOD of 0.5 mm.

Aidarov et al. [10] studied the effects of low temperatures on the flexural behavior of MSFRC. They observed an enhancement of the post-cracking behavior for temperature under 0 °C. Indeed, the residual tensile strength at CMOD of 0.5 mm and 2.5 mm increased up to 54% and 71% of the reference values at the room temperature of 20 °C. Richardson and Ovington [11] obtained consistent results about the improved strength at low temperatures. Pull-out tests showed a 50% increase of the pull-out force when the temperature is reduced from 60 °C to −20 °C.

* Corresponding author.
E-mail address: elisa.bassoli@unimore.it (E. Bassoli).

https://doi.org/10.1016/j.conbuildmat.2025.144385
Received 4 August 2025; Received in revised form 17 October 2025; Accepted 3 November 2025
Available online 5 November 2025

The thermal behavior of a composite material like PP-MSFRC depends on the properties of matrix and fibers together with their interactions. The main factor that affects the mechanical properties of concrete is the freezing of water inside its pores. Hence, the moisture content plays a major role for this aspect. Strength and stiffness of the concrete gradually increase up to moderate low temperature, about −30 °C [12,13]. As concerns positive temperatures, normal concrete mixes are usually characterized by a loss of strength and stiffness mainly caused by water migration, dehydration and inter-facial thermal incompatibility [14,15]. As far as PP is regarded, it is a thermoplastic semi-crystalline polymer that shows a large thermal sensitivity due to the low melting point. Its mechanical properties highly depends on its state, defined by two transition regions [16]. In addition, temperature effect on the fiber–matrix interaction has to be emphasized. The shrinkage of the concrete matrix at low temperatures determines an increase of the confinement pressure of the fibers and thus an improved anchorage capacity [17].

In the context of FRC modeling, a common strategy to determine the constitutive parameters is based on inverse analysis [18,19]. For example, tensile constitutive parameters can be calibrated on the basis of the experimental results of TPBTs [20,21]. Studies on the influence of temperature change on the model constitutive parameters are limited compared to the experimental counterpart [10,22] and the theme has to be further investigated. This work aims at studying the effect of temperature change on the constitutive parameters of a cracked hinge model, which are obtained by means of inverse analysis based on the results of TPBTs. Specimens are preserved at different temperatures (−30 °C, −15 °C, 0 °C, 20 °C, 40 °C and 60 °C) before the execution of the test. Moreover, a prediction model relating temperature and constitutive parameters is developed in the form of a hybrid regression model. This maintains the structure of a standard regression model, but numerical simulations of the mechanical model are embedded into the regression coefficient estimation. Different relationships between temperature and parameters, namely linear and bi-linear types, are studied and compared. The Akaike Information Criterion (AIC) is used as model selection criterion in order to select the more appropriate relationship [23]. The work aims at proposing a general strategy, that can be employed for different material properties, as the case of fibers characterized by different properties. For this reason, three groups of concrete specimens are considered, each one reinforced with different PP fibers. The results of TPBTs performed on these specimens are the basis for the development of three different prediction models, one for each fiber type. Analogies among the estimated prediction models are found, confirming the consistency of the proposed approach in the study of temperature effect on the parameters of different PP-MSFRC.

The paper is organized as follows: Section 2 describes the experimental campaign performed on the three specimen groups together with its results. Section 3 details the mechanical model adopted for the simulation of each experimental test and the procedure of inverse analysis. Section 4 presents the hybrid regression model that relates temperature and constitutive parameters, while its application to this case is shown in Section 5. Finally, conclusions are drawn in Section 6.

2. Experimental campaign

2.1. Materials and methods

The experimental campaign is carried out to characterize the temperature effect on the flexural behavior of three MSFRCs. Three different types of Polypropylene Macro Synthetic fibers (MSF) are employed; their properties are specified in Table 1, while Table 2 lists the concrete mix adopted. For MSFRC1 CEM I 52.5R is used as the fibers employed in this mixture are specifically designed for precast applications, where this type of cement is commonly adopted, for the other MSFRCs CEM II A-LL 42.5 R is used because the fibers used are for cast in place applications. The choice is therefore intended to reproduce typical industrial practice; however, the authors do not expect the type of cement to have a significant influence on the results presented in this study. Concrete is mixed using a vertical axis mixer, following the prescriptions of EN 14651 [24]. A polycarboxylic ether superplasticizer is used in all the mixes; its dosage adjusted to achieve a concrete consistency in class S3.

The campaign involves the execution of compression tests and TPBTs on specimens cured at different temperatures, namely −30 °C, −15 °C, 0 °C, 20 °C, 40 °C and 60 °C. The upper bound of the temperature range adopted in this study was selected to include realistic environmental conditions that fiber-reinforced concrete (FRC) structural elements may experience during their service life. The upper limit (+60 °C) represents the typical maximum temperature that may be reached by concrete surfaces or near-surface regions directly exposed to solar radiation, particularly in hot climates or under intense solar heating [25]. The lower limit (−30 °C) was chosen not only to represent exposure to severe cold climates but also to include the glass transition temperature T_g of polypropylene (approximately −10 °C [26]). This temperature represents a critical threshold for the mechanical performance of polymers even if polypropylene, being semi-crystalline, is more stable than amorphous polymers. In fact the crystalline phase provides structural rigidity that remains largely stable over a wide temperature range, while the amorphous phase undergoes a significant change in mechanical behavior around T_g. The temperature of 20 °C was selected to represent standard laboratory conditions and to provide baseline mechanical properties for comparison. Tests between 0 °C and 60 °C were performed at 20 °C intervals, while for sub-zero temperatures, an increment of 15 °C was adopted, as the environmental chamber used in the experimental campaign cannot operate below −30 °C. Compression tests are carried out on cubes with dimensions 150 mm × 150 mm × 150 mm, using 4 specimens per temperature. Before testing, specimens are cured for 25 days in water at 20 °C, then for one day at ambient temperature, and finally for two days in an environmental chamber at the target temperature.

As for TPBTs, eight specimens are tested for each MSFRC for each temperature. They have a size of 150 mm × 150 mm × 600 mm. After casting, TPBTs specimens are cured for 25 days in water at 20 °C, then a notch is sawed at mid span, with a depth of 25 mm and a thickness of 5 mm, as required by EN 14651; after notching the specimens are moved to an environmental chamber and exposed to the target test temperature for 48 h. The duration of the curing process is defined based on preliminary tests in which thermocouples were inserted inside a beam exposed to different temperatures. Fig. 1 depicts the positioning of the thermocouples within the mid-span notched cross-section. In addition, Fig. 1 illustrates the temperature readings from two sensors, obtained when the beam was subjected to a temperature of 59 °C, starting from an initial temperature of 22 °C. The air temperature sensor, denoted as T1, indicates that the environmental chamber requires approximately 5 h to attain the desired temperature. Conversely, the sensor T5, positioned within the beam, shows that the temperature within the cross-section reaches 95% of the target within approximately 9 h, while the target temperature is achieved in about 20 h. After curing the specimens are tested in TPB according to EN 14651. A clip-on displacement transducer is installed at the bottom of the specimen, across the notch, in order to measure the Crack Mouth Opening Displacement (CMOD). Test are carried out in CMOD control with an opening rate of 0.05 mm/min for CMOD ≤ 0.1 mm and 0.2 mm/min for CMOD > 0.1 mm, until a CMOD value of 4.0 mm is measured. Then, the displacement transducer is removed and the beam is tested to complete failure in displacement control, with a rate of 5 mm/min. A MTS servo-hydraulic testing machine is used to carry out the tests. The experimental setup is presented in Fig. 2. It is noted that tests are carried out at ambient temperature; however great care is taken in order to minimize the duration of the process after removing each specimen from the curing chamber, in order to reduce the temperature variation in the specimen. The entire

Table 1
Geometrical and mechanical properties of the fibers tested, as declared by the producer on the product label.

Property	MSF1	MSF2	MSF3
Equivalent diameter [mm]	0.81	0.85	0.70
Length [mm]	54	48	55
Aspect Ratio [-]	66.7	56.5	78.6
Tensile strength [MPa]	550	400	470
Modulus [GPa]	6.0	4.7	6.0
Melting point [°C]	160	160	160
Density [kg/m^3]	910	910	910

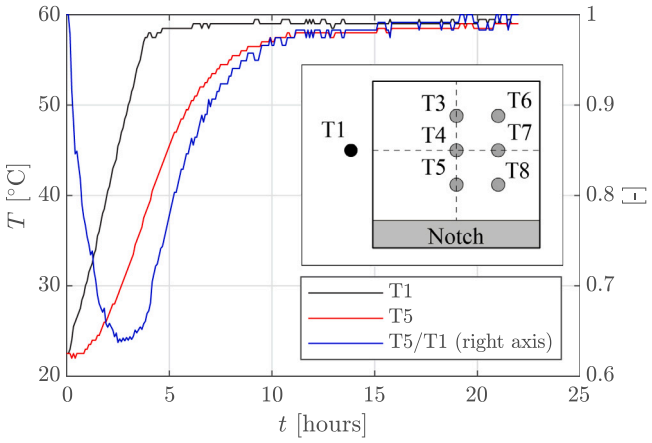

Fig. 1. Temperature distribution during curing at 59 °C for one of the beam specimens.

Fig. 2. The experimental setup for TPBT.

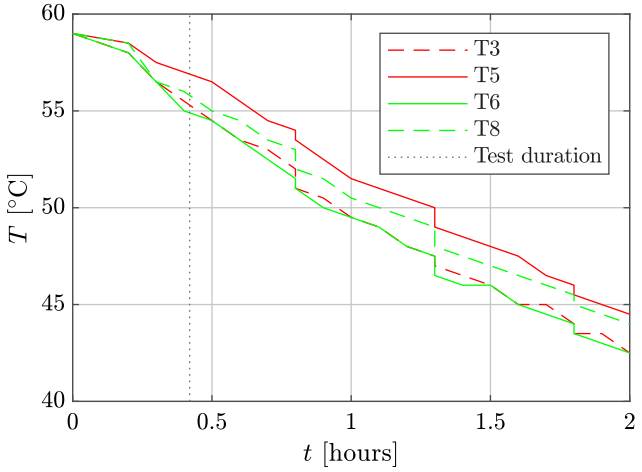

Fig. 3. Temperature changes in the specimen of Fig. 1 when exposed to an environmental temperature of 22 °C after curing for 48 h at 59 °C.

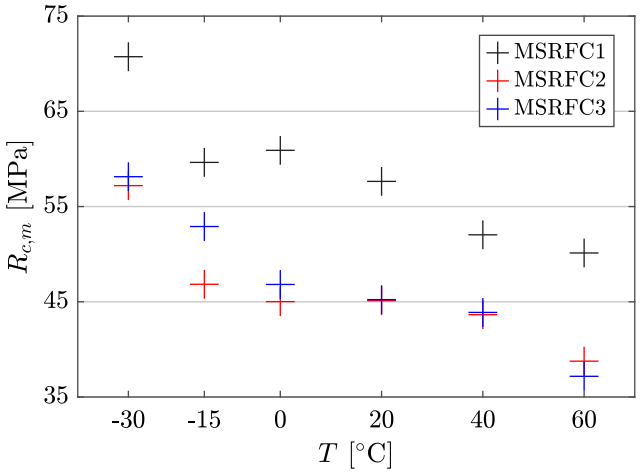

Fig. 4. Mean value of the concrete compression strength $R_{c,m}$ measured at different temperatures.

procedure takes less than 30 min. To better understand the temperature changes in the specimen during the tests, the same specimen used to collect the data reported in Fig. 1 is taken at environment temperature (22 °C), after curing for 48 h at 59 °C. The temperatures measured by the thermocouples are reported in Fig. 3. It is possible to notice that, within the test duration the variation of temperature measured by the thermocouple T5 (see Fig. 1 for the position) decreases by 2 °C while in the other positions by 4 °C. It is noted that at temperatures closer to the environment temperature a smaller variation is expected based on the Newton's law of cooling, which states that the rate of heat loss of a body is proportional to the difference the temperature between the body and the environment

2.2. Experimental results

Fig. 4 illustrates the mean values of the concrete compression strength measured at the different temperatures for the three materials tested. In general, excluding some limited fluctuations, it is possible to observe a monotonic variation of the strength with temperature; specifically the strength decreases as the temperature increases. This is consistent with the literature on plain concrete. The mean nominal stress vs. CMOD curve for each temperature is presented for MSFRC1, MSFRC2 and MSFRC3 in Fig. 5(a), Fig. 5(b) and Fig. 5(c), respectively. The three groups of curves show notable differences especially in the post peak region, mainly due to the different properties of the

Table 2
Concrete mix used for the MSFRCs tested.

Component	MSFRC1	MSFRC2	MSFRC3
CEM I 52.5 R [kg/m^3]	400.0	–	–
CEM A-LL 42.5 R [kg/m^3]	–	400	400
Fine Sand 0–1 mm [kg/m^3]	171.7	171.7	171.7
Sand 0–5 mm [kg/m^3]	729.5	729.5	729.5
Gravel 5–15 mm [kg/m^3]	836.8	836.8	836.8
Fiber type	MSF1	MSF2	MSF3
Fiber dosage [kg/m^3]	8.0	8.0	8.0
Water [L/m^3]	184.0	184.0	184.0
W/C ratio [-]	0.46	0.46	0.46

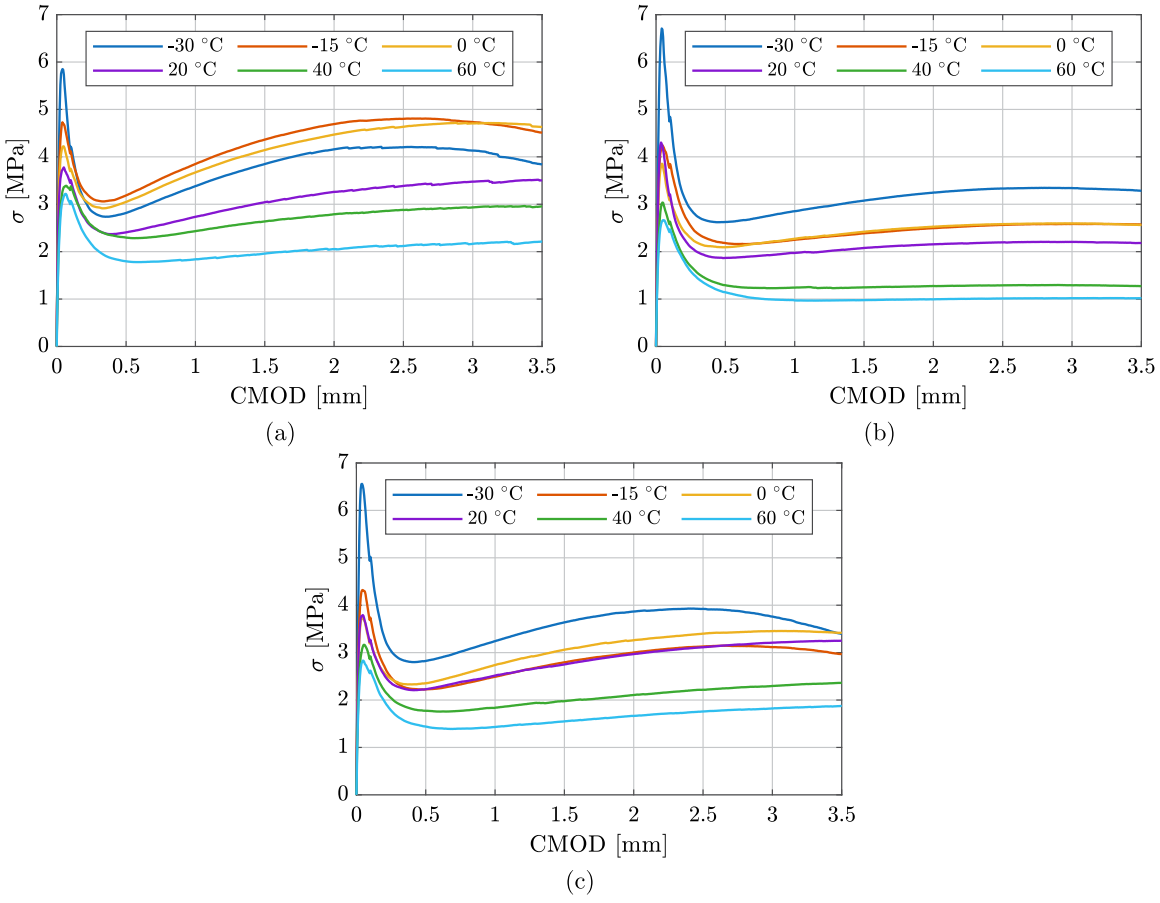

Fig. 5. Mean nominal stress vs. CMOD curves for groups of specimens tested at different temperatures: (a) MSFRC1, (b) MSFRC2, (c) MSFRC3.

fibers. However, similar features regarding the temperature effect on the specimen response can be observed, as discussed in the following. Considering the curve at 20 °C as reference, for all the materials tested higher temperatures lead to a strength decrease, while colder temperatures produce a strength increase. To better understand the effect of temperature, in the following the flexural tensile strength at the limit of proportionality ($f^f_{ct,L}$) and the nominal flexural residual tensile strengths at CMOD = 0.5 mm ($f_{R,1}$) and at CMOD = 2.5 mm ($f_{R,3}$) are analyzed in detail.

Fig. 6 presents $f^f_{ct,L}$ for the three MSFRCs subjected to testing. The crosses denote experimental outcomes, while the error bar highlights the interval defined by the mean tensile strength of the specimens tested at a specific temperature plus or minus one standard deviation. The right axis illustrates the ratio between the strength at temperature T and the strength at 20 °C. For all materials, it is evident that tensile strength increases as temperature decreases. The ratio of the strength at −30 °C to that at 20 °C is 1.54 for MSFRC1, 1.57 for MSFRC2, and 1.73 for MSFRC3. It is noted that the results at temperatures below 0 °C may be influenced by an ice-strengthening effect, which depends to the moisture content of the concrete [27–29].

At 60 °C, the strength ratio is 0.85, 0.62, and 0.74, respectively. It is noted that the trend is similar to that observed for the compression strength. Fig. 7 shows the values of $f_{R,1}$ and $f_{R,3}$ as a function of temperature for the three materials under consideration. The right axis indicates the ratio of the strength at a given temperature T, $f_{R,j}(T)$ (j = 1 or 3) to the mean strength at 20 °C, $\overline{f_{R,j}}$(20 °C). Analyzing this plot in contrast with Fig. 6, it becomes evident that the experimental results exhibit higher variability. Specifically, $f_{R,1}$ and $f_{R,3}$ are significantly influenced by the number of fibers crossing the crack, while $f^f_{ct,L}$ does not depend on the number of fibers for the materials under consideration. MSFRC2 and MSFRC3 demonstrate a nearly linear decrease in $f_{R,j}(T)$ (j = 1 or 3) as temperature increases. Conversely, MSFRC1 deviates from this linear trend at lower temperatures.

To verify the variability attributed to the fiber distribution, a fiber count was conducted at the conclusion of the bending tests. The crack surface was divided into three horizontal strips of equal height, and

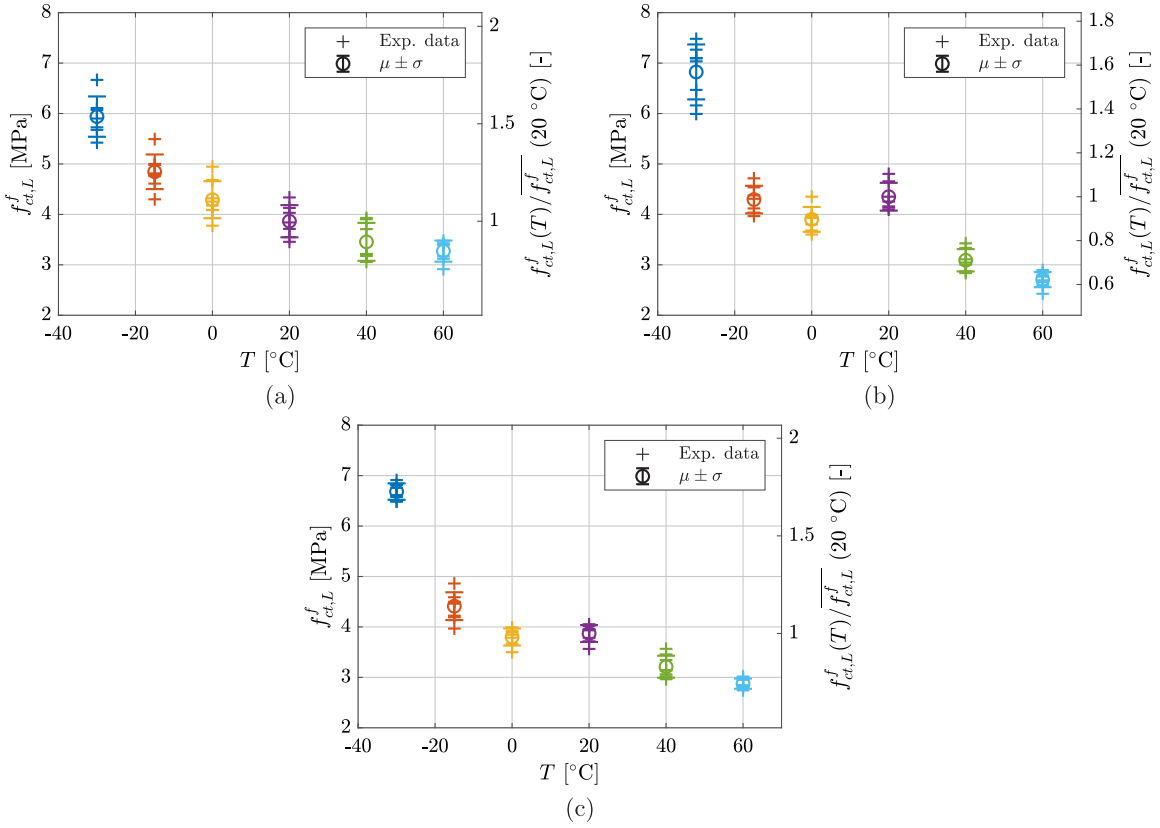

Fig. 6. Flexural tensile strength at the limit of proportionality [24] for all the specimens tested: (a) MSFRC1; (b) MSFRC2; (c) MSFRC3. The left axis indicates actual strength values $f^f_{ct,L}$ while the right axis indicates the ratio between the strength at temperature T ($f^f_{ct,L}(T)$) and the mean strength at 20 °C ($\overline{f^f_{ct,L}}$(20 °C)).

fibers were distinguished between broken and pulled-out fibers. In the following the number of fibers in the two bottom strips ($N_{F,12}$) is considered, because previous works have shown that it has a good correlation with the residual strength [30,31]. Fig. 8 shows an example of the correlation between the number of fibers and the residual strength $f_{R,3}$ for MSFRC3. Fig. 9 illustrates $N_{F,12}$ for all tested specimens. The dots represent experimental data, while crosses indicate the mean number of fibers on the specimens tested at the specified temperature T. The dashed horizontal lines represent the mean number of fibers computed considering all specimens for each MSFRC. Generally, the variability is substantial, as anticipated, and appears particularly pronounced for MSFRC2, where the mean number of fibers exhibits significant deviations from the mean value at certain temperatures. Finally, Fig. 10 presents the ratio between the pulled-out fibers and the broken fibers observed during the fiber counting at the conclusion of the bending tests. The plot indicates that as the temperature rises, the number of pulled-out fibers tends to increase, while the number of broken fibers decreases. This observation aligns with the variation of the elastic modulus of Polypropylene as the temperature increases [16,32], as this parameter plays a pivotal role in determining the pull-out behavior of fibers.

3. Cracked hinge model

A cracked hinge model is employed to simulate the behavior of MSFRCs. The fundamental concepts of the model have been introduced in [33] and are summarized in the following. The non-linearity due to the presence of cracks takes place in a hinge of finite length (denoted as s) that is delimited by rigid boundaries. Olesen [33] suggests to set the hinge length to half of the section height, based on comparison with nonlinear finite-element calculations, and on findings from Ulfkjær et al. [34]. Independent horizontal springs arranged in layers and attached at each end to the rigid boundary constitute the hinge. Outside the boundaries, the behavior is that of an un-cracked element. For this reason, the model is well suited for the simulation of an experimental test where the crack triggering is controlled, as for those involved in the present work .

The non-linear behavior of each spring layer is defined as:

$$\sigma(w) = \begin{cases} E\epsilon & \text{if } w = 0 \\ g(w)\, f_{ct} & \text{if } w > 0 \end{cases} \tag{1}$$

where E is the elastic modulus of concrete, ϵ is the elastic strain, f_{ct} is the tensile strength of concrete, w is the crack opening and $g(w)$ represents the stress-crack opening relationship normalized with respect to f_{ct}.

The choice of the type of relationship influences the model response and it was analyzed by several authors. A good trade-off between accuracy and simplicity can be obtained by multi-linear relationships. In this way, an analytical formulation for the simulation of the flexural behavior of concrete can be exploited [35]. It was shown in [36] that a bi-linear relationship is unsatisfactory in reproducing with accuracy a strain-hardening type response and it is suggested the use of tri-linear o tetra-linear relationships.

In this work, a tri-linear relationship has been selected :

$$g(w) = \begin{cases} 1 + b_1 w & \text{if } 0 \le w \le w_1 \\ a_2 + b_2 w & \text{if } w_1 < w \le w_2 \\ a_3 + b_3 w & \text{if } w_2 < w \le w_3 \end{cases} \tag{2}$$

where $g(w_3) = 0$. The graphical representation of the trilinear stress-crack opening relationship is reported in Fig. 11. The force-CMOD curve resulting from a TPBT can be obtained through a numerical procedure, for which it is convenient to vary the average curvature of the hinge inside a range of values determined with engineering judgment. For

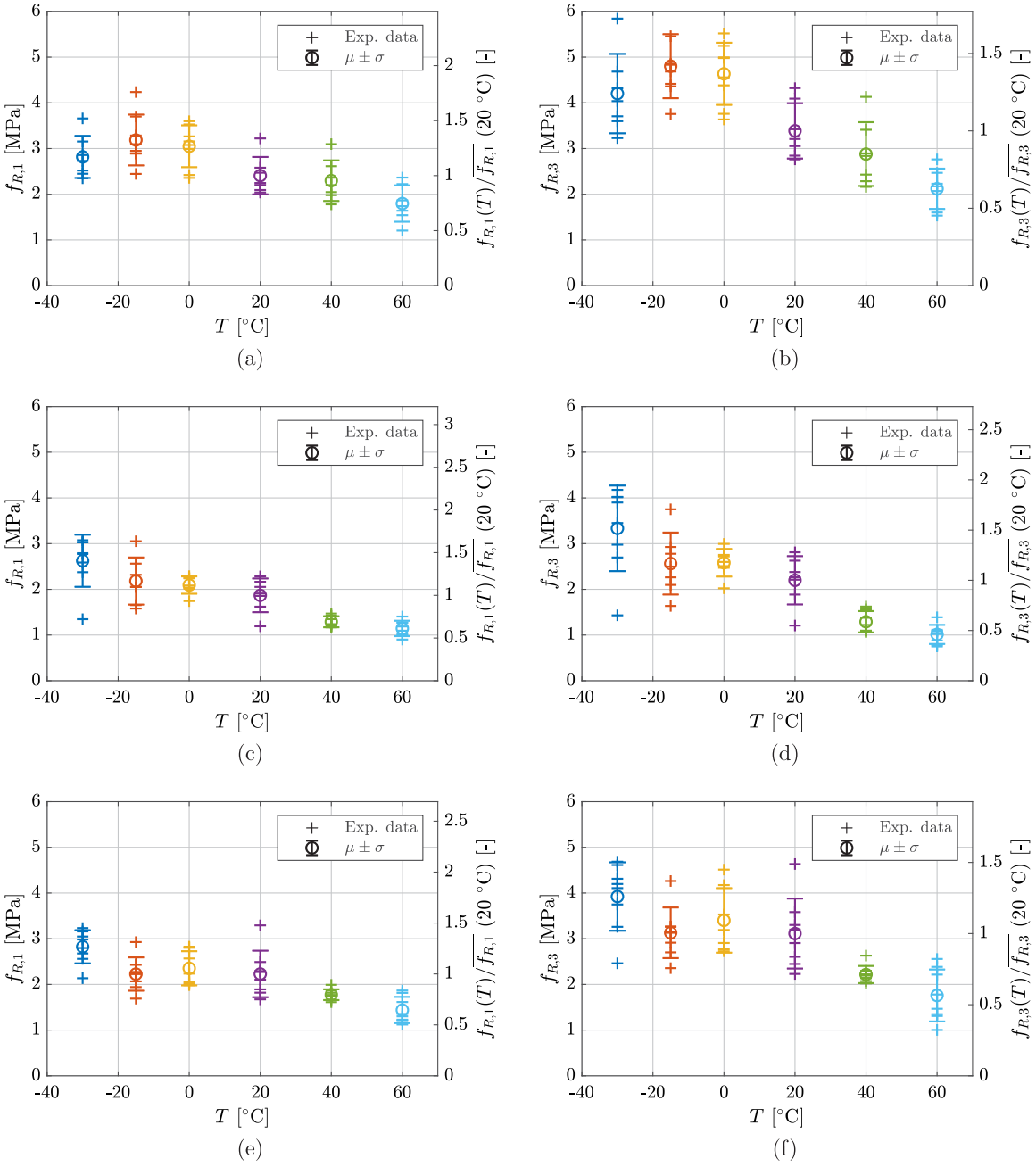

Fig. 7. Residual flexural tensile strengths $f_{R,1}$ and $f_{R,3}$ for all the specimens tested: (a,b) MSFRC1, (c,d) MSFRC2 and (e,f) MSFRC3. The left axis indicates actual strength values $f_{R,j}$ while the right axis indicates the ratio between the strength at temperature T ($f_{R,j}(T)$) and the mean strength at 20 °C ($\overline{f_{R,j}}$(20 °C)). $j = 1$ for (a,c,e) and $j = 3$ for (b,d,f).

each value of the average curvature, the force and CMOD values can be computed by combining kinematic compatibility, force equilibrium and constitutive law of the hinge. Due to the piece-wise linear stress-crack opening relationship, the solution can be achieved numerically or in a closed-form expression by defining transition values for the average curvature that represent the transition from a segment of the stress-crack opening relationship to the following one. More details can be found in [37].

3.1. Inverse analysis

The constitutive parameters defining the structural behavior (Eqs. (1)-(2)) are usually calibrated by means of inverse analysis. As regards the tri-linear stress-crack opening relationship, it is possible to directly calibrate the parameters that appear in Eq. (2), namely b_1, a_2, b_2, a_3, b_3, w_1, w_2 and w_3. A better choice is to consider $g(w_1)$ and $g(w_2)$ instead of the intercepts and the slopes of the three lines, since these latter are related to each others. Moreover, it is easier to bound $g(w_1)$ and $g(w_2)$. For these reasons, we consider the parameters f_{ct}, w_1, $g(w_1)$, w_2, $g(w_2)$, w_3. The aim of the inverse analysis is to tune their values in order to have a model simulation that best approximates an experimental test. The force-CMOD curve resulting from an experimental test can be symbolically described by the function F_{exp}(CMOD) that gives the force value for a generic CMOD. In analogy, the curve simulated by the mechanical model is denoted as F_{num}(CMOD). The inverse analysis is carried out by solving an optimization problem aimed at minimizing an error function that measures the discrepancy between F_{exp}(CMOD) and F_{num}(CMOD). The calibrated parameters are those that allow to

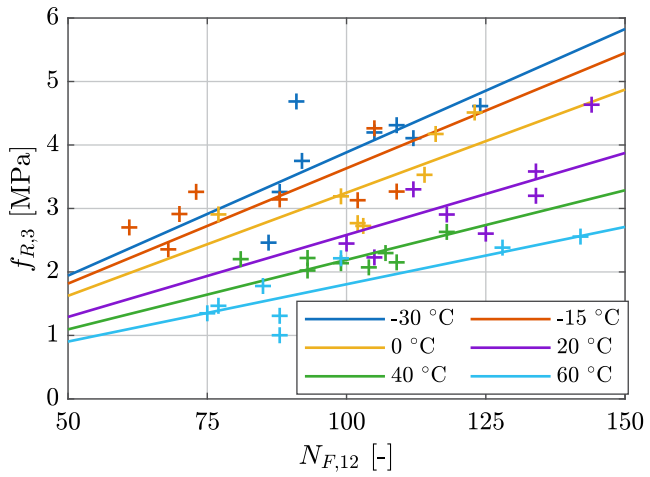

Fig. 8. Correlation between the number of fibers $N_{F,12}$ and the residual strength $f_{R,3}$ for MSFRC3.

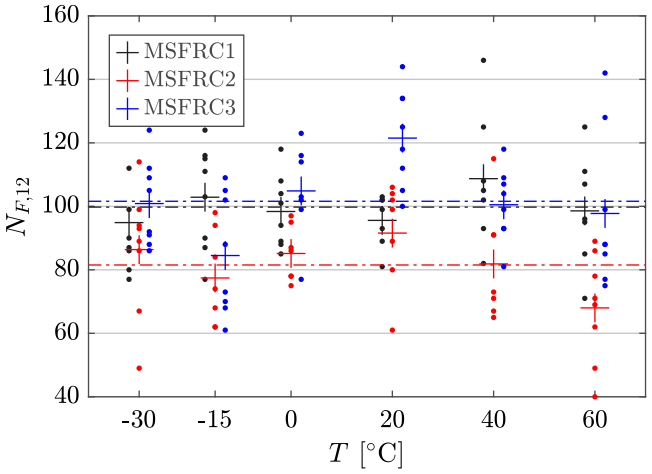

Fig. 9. Number of fibers crossing the bottom two thirds of the crack section ($N_{F,12}$) for all the specimens tested.

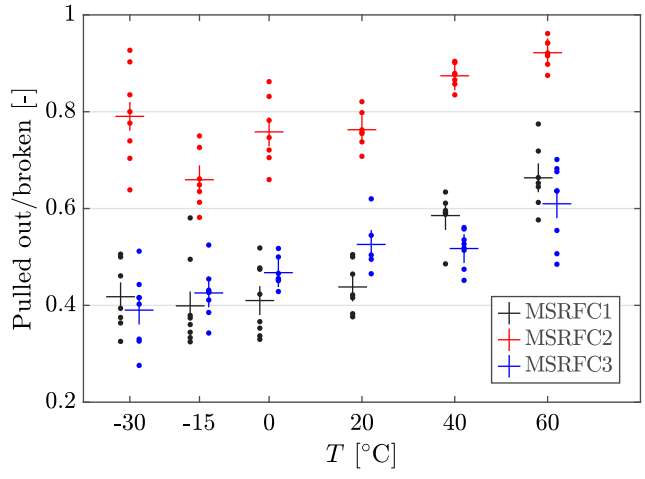

Fig. 10. Ratio of pulled out over broken fibers for all the specimens tested.

have the minimum value of the error function. The choice of the error function is motivated by the necessity to have a common measure of discrepancy that is effective for curves that can be very different among

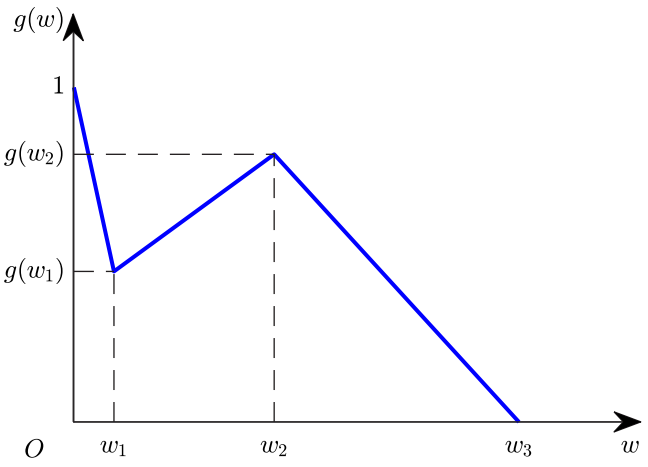

Fig. 11. Trilinear normalized stress-crack opening relationship.

each other (see Fig. 5 for example). Hence, the error function J is expressed as:

$$J(\mathbf{x}) = \int_0^{C_{max}} \psi\,(\mathrm{CMOD})\left[F_{num}\,(\mathrm{CMOD},\mathbf{x}) - F_{exp}\,(\mathrm{CMOD})\right]^2 \mathrm{dCMOD} \quad (3)$$

where C_{max} is the maximum value of CMOD reached in the experimental test,

$$\mathbf{x} = \left[f_{ct}, w_1, g\,(w_1), w_2, g\,(w_2), w_3\right] \quad (4)$$

contains the calibration parameters and ψ (CMOD) is a weighting function that gives more importance to the peak region of the force-CMOD curve compared to the other regions. It has been shown in other works [36,38] that a similar approach is necessary in order to simulate with accuracy the behavior of fiber reinforced concrete when large range of crack openings are considered. The weighting function is defined as:

$$\psi\,(\mathrm{CMOD}) = \begin{cases} \dfrac{\bar{\psi}}{\bar{C}}\mathrm{CMOD} & \text{if } 0 \le \mathrm{CMOD} \le \bar{C} \\ 2\bar{\psi} - \dfrac{\bar{\psi}}{\bar{C}}\mathrm{CMOD} & \text{if } \bar{C} < \mathrm{CMOD} \le \dfrac{2\bar{\psi}-1}{\bar{\psi}}\bar{C} \\ 1 & \text{if } \dfrac{2\bar{\psi}-1}{\bar{\psi}}\bar{C} < \mathrm{CMOD} \le C_{max} \end{cases} \quad (5)$$

$\bar{C}$ is the CMOD value corresponding to the peak of F_{exp} and $\bar{\psi}$ is the weight associated to the peak (equal to 50 in this application). An illustration of the weighting function is depicted in Fig. 12. The curves involved in Eq. (3) are defined by discrete quantities, therefore the integral needs to be numerically evaluated by means of the trapezoidal rule.

It is recommended to devise some expedients in order to simplify the optimization process. First, the parameter w_2 is substituted by $\Delta w_{1-2} = w_2 - w_1$ in order to avoid the adoption of additional constraints. Second, it was already pointed out [21] that the error function is not sensitive to the variation of the w-coordinate of the last point, w_3 in this work, beyond values larger than C_{max}. For this reason, a better solution is to calibrate the stress value corresponding to a crack opening value $\bar{w}$ smaller than C_{max}, namely $g\,(\bar{w})$. In this work, it is chosen $\bar{w} = 3$ mm. It should be noticed that the elastic modulus of the concrete is not included into the calibration because it has a very limited effect on the force-CMOD curve after the first peak. A value of 37200 MPa is used.

The minimization of the error function J can be a complex task for the large dimension of the parameter space (i.e. 6) and for the use of experimental data. The optimization is conducted with an improved evolutionary algorithm [39]. It combines the robustness in the search of the global minimum that is typical of evolutionary algorithms with a local second-order surrogate of the error function and a proper sampling strategy. The improved algorithm requires a reduced number

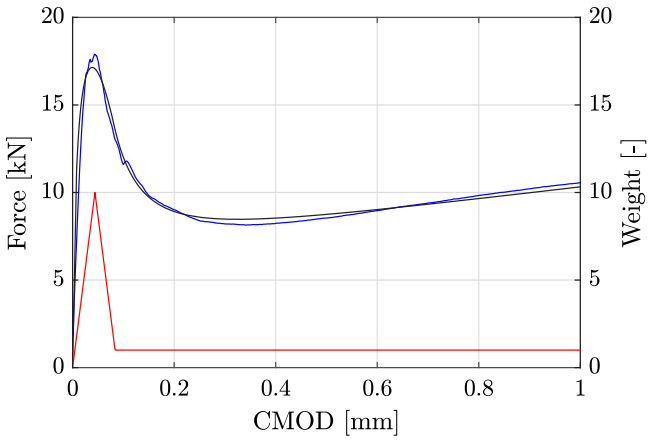

Fig. 12. Weighting function (red) using $\bar{\psi} = 10$ associated to the experimental force-CMOD curve (blue) and the corresponding calibrated numerical simulation (black).

of evaluations compared to a traditional evolutionary algorithm and at the same time it maintains a comparable accuracy.

4. Temperature effect on model parameters

The present section delineates a procedure for the development of a prediction model relating temperature and constitutive parameters of the cracked hinge model (see Section 3). In general terms, the relationship between temperature T and the ith parameter of the cracked hinge model x_i is described as a regression model:

$$x_i = h_i\left(T, \boldsymbol{\beta}_i\right) + e \qquad i = 1, \dots, N_p \tag{6}$$

where x_i is the response variable. h_i represents the regression model for each response variable x_i, $\boldsymbol{\beta}_i$ is the vector collecting the regression model coefficients and e is an additive error term. The specific form of each regression model h_i will be defined later. N_p is the number of model parameters and for each of these the coefficient vector $\boldsymbol{\beta}_i = \left[\beta_{i,1}, \dots, \beta_{i,n_i}\right]$ is different. Note that also the number of coefficients n_i for each mechanical parameter x_i can be different. The totality of the coefficients to be estimated can be denoted as $\boldsymbol{\theta} = \left[\boldsymbol{\beta}_1, \dots, \boldsymbol{\beta}_i, \dots, \boldsymbol{\beta}_{N_p}\right]$. In this regard, a common approach involves the determination of the coefficients in a least square sense by exploiting known values of predictor and response variable. For the latter, known values are not directly measured but derived through model inversion based on the results of each tested specimen, following the procedure of Section 3.1. However, the presence of outliers in the data and the errors introduced by the inverse analysis can negatively influence the coefficient estimation performed with the ordinary least square method.

A more robust approach does not involve the inversion of the mechanical in a previous phase and the subsequent fitting of the regression model, but it embeds model simulations in a unique phase of regression coefficient estimation [40]. In this case, all the regression coefficients $\left[\boldsymbol{\beta}_1, \dots, \boldsymbol{\beta}_i, \dots, \boldsymbol{\beta}_{N_p}\right]$ are simultaneously estimated by minimizing a global error function J_{gl} defined as:

$$J_{\text{gl}}(\boldsymbol{\beta}_1, \dots, \boldsymbol{\beta}_i, \dots, \boldsymbol{\beta}_{N_p}) = \sum_{j=1}^{N_T} \sum_{k=1}^{N_{\text{sp}}} J\left[\mathbf{x}\left(\boldsymbol{\beta}_1, \dots, \boldsymbol{\beta}_i, \dots, \boldsymbol{\beta}_{N_p}\right)\right] \tag{7}$$

where J has been defined in Eq. (3) for the inverse analysis based on a single specimen, N_T is the number of different temperatures considered in the experimental campaign and N_{sp} is the number of specimens preserved at each temperature. The dependence of $\mathbf{x}$ on the regression coefficients is expressed in an implicit form in Eq. (6). Another advantage of the proposed hybrid approach is that the global error function of Eq. (7) has also a regularizing task, since the predicted parameters have a physical meaning for the temperature values adopted in the calibration. This is not ensured by the former approach.

5. Results

The procedure delineated in Section 4 is applied to the data obtained by the experimental campaign of Section 2. The aim is to assess the temperature effect on the constitutive parameters of MSFRCs and to develop a prediction model. Moreover, the selection of the most adequate prediction model that fits the relationship between temperature and constitutive parameters is investigated. Four regression models are studied and their specifications are listed in Table 3. $\mathcal{M}_1$ involves a linear relationship between each one of the six parameters of the cracked hinge model and temperature, for a total of 12 coefficients. With reference to the generic form of Eq. (6), it is possible to write:

$$\mathcal{M}_1 : \begin{cases} x_1 = f_{ct} & h_1 = \beta_{1,1} + \beta_{1,2}T \\ x_2 = w_1 & h_2 = \beta_{2,1} + \beta_{2,2}T \\ x_3 = g\left(w_1\right) & h_3 = \beta_{3,1} + \beta_{3,2}T \\ x_4 = \Delta w_{1-2} & h_4 = \beta_{4,1} + \beta_{4,2}T \\ x_5 = g\left(w_2\right) & h_5 = \beta_{5,1} + \beta_{5,2}T \\ x_6 = g\left(\bar{w}\right) & h_6 = \beta_{6,1} + \beta_{6,2}T \end{cases} \tag{8}$$

$\mathcal{M}_2$, $\mathcal{M}_3$ and $\mathcal{M}_4$ consider a bi-linear relationship for each parameter. $\mathcal{M}_2$ is the most general and it assumes different coefficients for each parameter:

$$\mathcal{M}_2 : \begin{cases} x_1 = f_{ct} & h_1 = \begin{cases} \beta_{1,1} + \beta_{1,2}T & \text{if } T \le \beta_{1,4} \\ q_1 + \beta_{1,3}T & \text{if } T > \beta_{1,4} \end{cases} \\ x_2 = w_1 & h_2 = \begin{cases} \beta_{2,1} + \beta_{2,2}T & \text{if } T \le \beta_{2,4} \\ q_2 + \beta_{2,3}T & \text{if } T > \beta_{2,4} \end{cases} \\ x_3 = g\left(w_1\right) & h_3 = \begin{cases} \beta_{3,1} + \beta_{3,2}T & \text{if } T \le \beta_{3,4} \\ q_3 + \beta_{3,3}T & \text{if } T > \beta_{3,4} \end{cases} \\ x_4 = \Delta w_{1-2} & h_4 = \begin{cases} \beta_{4,1} + \beta_{4,2}T & \text{if } T \le \beta_{4,4} \\ q_4 + \beta_{4,3}T & \text{if } T > \beta_{4,4} \end{cases} \\ x_5 = g\left(w_2\right) & h_5 = \begin{cases} \beta_{5,1} + \beta_{5,2}T & \text{if } T \le \beta_{5,4} \\ q_5 + \beta_{5,3}T & \text{if } T > \beta_{5,4} \end{cases} \\ x_6 = g\left(\bar{w}\right) & h_6 = \begin{cases} \beta_{6,1} + \beta_{6,2}T & \text{if } T \le \beta_{6,4} \\ q_6 + \beta_{6,3}T & \text{if } T > \beta_{6,4} \end{cases} \end{cases} \tag{9}$$

The intercept for the second line of the generic parameter x_i is $q_i = \beta_{i,1} + \beta_{i,4}\left(\beta_{i,2} - \beta_{i,3}\right)$. Since a single bi-linear relationship is defined by 4 coefficients, $\mathcal{M}_2$ has 24 in total. $\mathcal{M}_3$ assumes that the transition temperature, namely the temperature value determining the transition from a line to the other, is the same for 5 parameters (w_1, $g\left(w_1\right)$, Δw_{1-2}, $g\left(w_2\right)$, $g\left(\bar{w}\right)$) and it is different only for f_{ct}. By referring to the terminology of Eq. (9), it means that $\beta_{2,4} = \beta_{3,4} = \beta_{4,4} = \beta_{5,4} = \beta_{6,4}$. Finally, $\mathcal{M}_4$ supposes a single transition temperature, that is equal for all the six parameters ($\beta_{1,4} = \beta_{2,4} = \beta_{3,4} = \beta_{4,4} = \beta_{5,4} = \beta_{6,4}$). Hence, $\mathcal{M}_3$ and $\mathcal{M}_4$ have 20 and 19 coefficients, respectively.

Each regression model is the component of a hybrid regression model whose coefficients are determined by minimizing the error function of Eq. (7). The minimization is carried out by means of the improved evolutionary algorithm introduced in Section 3.1.

The estimated coefficients of the hybrid models are presented in Table 4 and the corresponding relationships are compared for each parameter in Fig. 13. We present only the results for MSFRC3 because they are similar to those of MSFRC1 and MSFRC2, which does not add further observations. Black dots in Fig. 13 represent the parameter values obtained with the inverse analysis based on each single experimental force-CMOD curve. Red asterisks are the mean value computed among the parameters associated to the same temperature. A simple

Table 3
Analyzed regression models.

ID	Relationship	nr. of coefficients (K)	Spec.
$\mathcal{M}_1$	Linear	12	–
$\mathcal{M}_2$	Bi-linear	24	6 transition temp.
$\mathcal{M}_3$	Bi-linear	20	2 transition temp.
$\mathcal{M}_4$	Bi-linear	19	1 transition temp.

visual analysis of these data, performed before the development of the prediction models, reveals that the bi-linear relationship can fit very well the mean values, except for w_1 (Fig. 13(b)) and Δw_{1-2} (Fig. 13(d)). As concerns the estimated regression models, linear relationships largely differ from the others and are not well suited to describe the dependency between the constitutive parameters and temperature.

$\mathcal{M}_2$ and $\mathcal{M}_3$ result in very similar relationships, almost identical for some parameters, for example f_{ct} (Fig. 13(a)) and $g\left(w_2\right)$ (Fig. 13(e)). This is confirmed by the very limited difference among the estimated coefficients listed in Table 4. Slightly larger differences are found for w_1 (Fig. 13(b)) and Δw_{1-2} (Fig. 13(d)), for which the fit with the mean values at each temperature is not accurate. However, this does not determine a large discrepancy between the predicted curves, as it will be shown in the following. On the other hand, $\mathcal{M}_4$ has estimated coefficients characterized in some cases by different order of magnitudes compared the corresponding ones of $\mathcal{M}_2$ and $\mathcal{M}_3$, for example $\beta_{3,3}$, $\beta_{4,2}$, $\beta_{4,3}$, $\beta_{5,3}$ and $\beta_{6,3}$. As a consequence, $\mathcal{M}_4$ gives different relationships compared to those of the other bi-linear models for most of the parameters. This is motivated by the unique transition temperature for all the parameters in the model.

The force-CMOD curves predicted by the competing hybrid models are compared to the average experimental curves of MSFRC3 for each temperature in Fig. 14. In analogy with the previous considerations, the curves predicted by $\mathcal{M}_1$ are in general the most distant from the experimental target. $\mathcal{M}_2$ and $\mathcal{M}_3$ predict curves that are practically overlapped for each temperature. The discrepancies observed in Figs. 13(b) and 13(d) for the relationships T-w_1 and T-Δw_{1-2} given by $\mathcal{M}_2$ and $\mathcal{M}_3$ do not cause differences in the model response. It is due to the low sensitivity of the cracked hinge model to variations of the these parameters in the ranges reported in Figs. 13(b) and 13(d). The predicted curves are in high accordance with the experimental ones, with only limited deviations for the temperatures of 20 °C (Fig. 14(d)) and 40 °C (Fig. 14(e)). The curves of $\mathcal{M}_4$ shows large discrepancies especially for the temperature of −15 °C (Fig. 14(b)), 20 °C (Fig. 14(d)) and 60 °C (Fig. 14(f)), confirming how the use of a unique transition temperature for all the parameters is an excessive simplification. In analogy to Fig. 13, the comparison for MSFRC1 and MSFRC2 is not presented but the observations are similar.

5.1. Regression model selection

The accuracy of the estimated prediction model is directly related to the regression model, namely to the type of function h used in Eq. (6) to describe the relationship. A priori evaluation of the more adequate function is not an easy task due to the complexity of the procedure. A practical approach involves the comparison of different competing models and the selection of the more appropriate one. This can be carried out according to a measure of model quality. In this work we use the Akaike Information Criterion (AIC) [23]. It is an information-theoretic selection criterion based on the Kullback–Leibler information theory [41]. Starting from the assumption that the best model is the one that minimizes the information loss, Akaike proposed to approximate the relative Kullback–Leibler information as:

$$\mathrm{AIC} = -2\log\left(\mathcal{L}\left(\hat{\boldsymbol{\theta}}|\mathbf{D},\mathcal{M}\right)\right) + 2K \tag{10}$$

where $\mathcal{L}\left(\hat{\boldsymbol{\theta}}|\mathbf{D},\mathcal{M}\right)$ is the maximum of the likelihood function for the dataset $\mathbf{D}$ and the model $\mathcal{M}$. $\hat{\boldsymbol{\theta}}$ is the value of the coefficient vector $\boldsymbol{\theta}$, introduced in Section 4, that maximizes the likelihood function and $2K$ is a bias correction depending on the dimension of $\hat{\boldsymbol{\theta}}$, namely the number of model coefficients. In [42] it is introduced a second-order bias correction to be used when the ratio between dataset dimension (N) and the number of model coefficients (K) is small:

$$\mathrm{AIC_C} = -2\log\left(\mathcal{L}\left(\hat{\boldsymbol{\theta}}|\mathbf{D},\mathcal{M}\right)\right) + 2K + \frac{2K\left(K+1\right)}{N-K-1} \tag{11}$$

The following simplified expression is obtained by assuming a Gaussian likelihood function and by approximating its variance with the sample variance of the datasets [43]:

$$\mathrm{AIC_C} = N\left(1+\log 2\pi\right) + N\log\left[\frac{1}{N}\sum_{t=1}^{N}\epsilon_t^2\left(\hat{\boldsymbol{\theta}}\right)\right] + 2K + \frac{2K\left(K+1\right)}{N-K-1} \tag{12}$$

where ϵ_t is the prediction error defined as the difference between the tth dataset and the model prediction for $\hat{\boldsymbol{\theta}}$. The best model among those compared is associated to the minimum value of $\mathrm{AIC_C}$.

For the present application, models to be compared are hybrid regression models combining the cracked hinge model and different regression models that will be described in Section 5. Hence, $N = N_T \cdot N_{\mathrm{sp}}$. Finally, it can be proved that $\frac{1}{N}\sum_{t=1}^{N}\epsilon_t^2\left(\hat{\boldsymbol{\theta}}\right)$ can be related to the minimum value of the error function J_{gl} of Eq. (7). Model performances for each material, measured by the error function J_{gl} and the $\mathrm{AIC_C}$ values, are compared in Table 5. As concerns J_{gl}, the same consideration holds independently on the MSFRC type. The minimum of the error function J_{gl} is always obtained by $\mathcal{M}_2$, the most complex model in terms of coefficient number. $\mathcal{M}_1$ has larger values, while the value of $\mathcal{M}_3$ is always very close to the minimum. If the $\mathrm{AIC_C}$ values are concerned, the results are different: the minimum value for MSFRC1 is obtained by $\mathcal{M}_4$, even if the value of $\mathcal{M}_3$ is very close, and the minimum for MSFRC2 and MSFRC3 is obtained by $\mathcal{M}_3$. $\mathcal{M}_3$ and $\mathcal{M}_4$ assume the same relationship type of $\mathcal{M}_2$ for the parameters of the cracked hinge model, namely a bi-linear type, but they have a reduced number of coefficients due to specific simplifications. This is the reason why they are the best models ($\mathcal{M}_4$ for MSFRC1, $\mathcal{M}_3$ for MSFRC2 and MSFRC3) according to the Akaike Information Criterion, that searches a trade-off between accuracy and simplicity.

5.2. Variation of the constitutive parameters with temperature for the selected model

The authors believe that $\mathcal{M}_3$ can be assumed as the reference model for the definition of the temperature effect on cracked hinge model parameters. Indeed, it is the most adequate model for MSFRC2 and MSFRC3 according to the AIC criterion, and for MSFRC1 the $\mathrm{AIC_C}$ value is very close to the minimum obtained by $\mathcal{M}_4$. Its predictions are in high accordance with the experimental data and they are practicality the same of model $\mathcal{M}_2$, which however has a higher number of coefficients. $\mathcal{M}_3$ is well suited to describe the temperature dependency for all the MSFRCs considered in the experimental campaign, highlighting the consistency of the proposed approach towards different materials properties. Considering the aim of this work, namely the study of temperature effects on the constitutive parameters of a design-oriented model, the use of two transition temperatures can be justified by physical considerations related to the thermal behavior of its constituent materials. Polypropylene has a melting temperature of 160 °C, and it is more strongly affected by temperature variations than concrete. Moreover, the glass transition usually lies in the range between −20 °C and +40 °C, depending on the type of polypropylene [16,26,32]. When

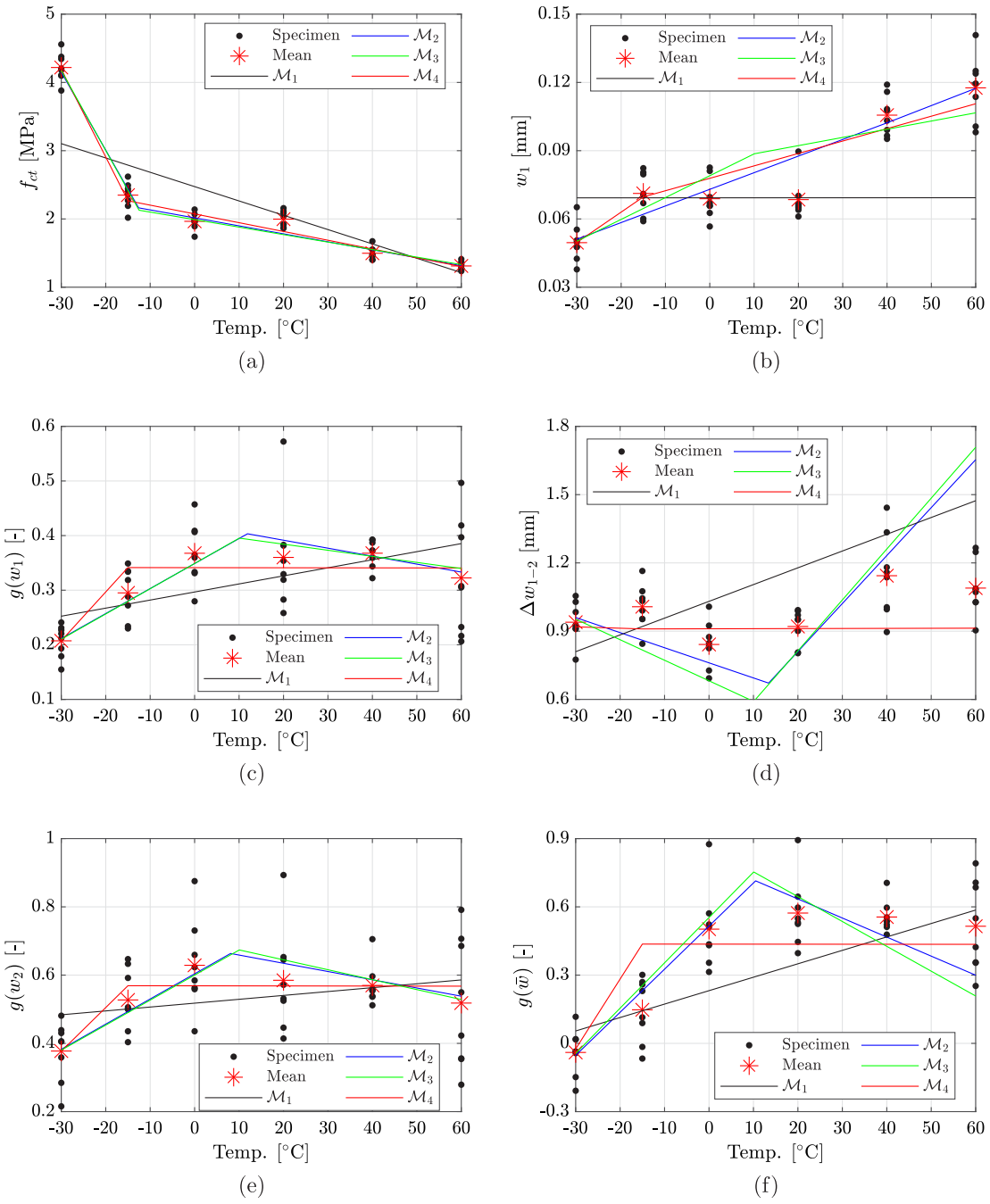

Fig. 13. Comparison among the different regression models for MSFRC3. Black dots: results of the inverse analysis for each tested specimen. Red asterisk: mean over the same temperature value. Line colors: black-$\mathcal{M}_1$, blue-$\mathcal{M}_2$, green-$\mathcal{M}_3$ and red-$\mathcal{M}_4$.

this phenomenon occurs, an increasing proportion of the material goes to a rubbery or viscous stage, thereby reducing stiffness and strength of the material [44]. Therefore it is deemed appropriate to use a transition temperature for the parameters primarily associated with the post-cracking behavior that is different from the transition temperature for f_{ct}.

Fig. 15 shows the variation of the tri-linear stress-crack opening relationship induced by temperature change in the interval [−30 60] ° C for the three MSFRCs. Figs. 15(a), 15(c) and 15(e) present the constitutive relationship in a large range of crack opening (0–4 mm), whereas Figs. 15(b), 15(d) and 15(f) are focused on the range 0–0.2 mm in order to better highlight the differences induced by temperature changes for the parameters f_{ct} and w_1. It can be stated that the modification of the constitutive relationship induced by temperature ranging in the interval [−30 60] ° C is remarkable for all the MSFRCs and it has a substantial influence on the model response. Common trends are observed for all the MSFRCs. f_{ct} has a decreasing trend with temperature. It is consistent with the behavior observed by other authors, characterized by a ice-strengthening effect at temperatures below 0 °C [11,12] and by the loss of strength and stiffness of normal concrete mixes mainly caused by water migration, dehydration and inter-facial thermal incompatibility [14,15]. w_1 increases with temperature, reflecting a rightward shift of the valley in the force-CMOD curve, accompanied by a reduction in the corresponding stress value $\sigma(w_1) = g(w_1) \cdot f_{ct}$. A similar trend is observed for w_2 which defines the CMOD location of the second peak of the curve and its associated stress $\sigma(w_2) = g(w_2) \cdot f_{ct}$. Parameter w_3 shows a marked increase between

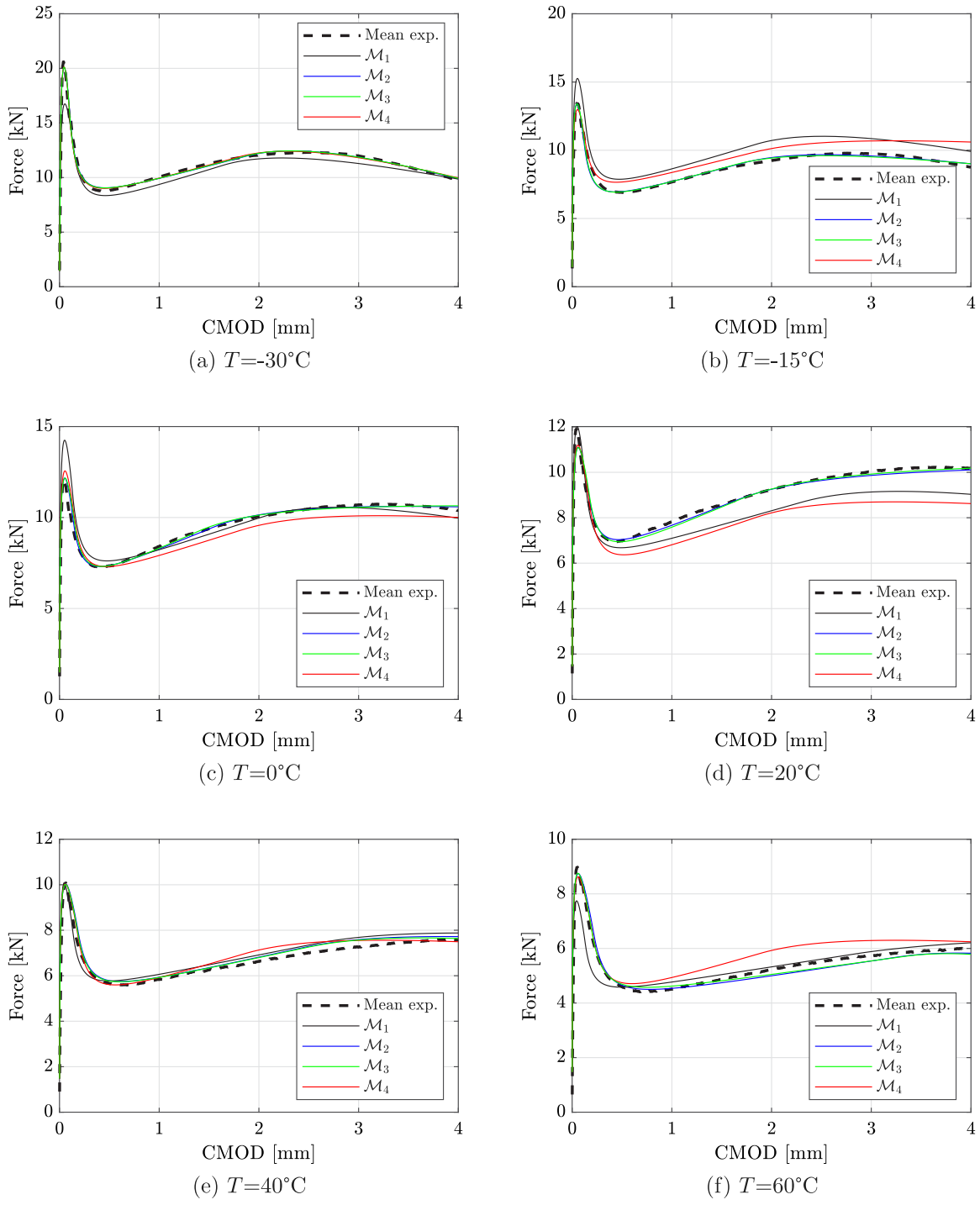

Fig. 14. Comparison among the average experimental curve (dashed black line) at each considered temperature with the numerical predictions of the different regression models for MSFRC3. Line colors: black-$\mathcal{M}_1$, blue-$\mathcal{M}_2$, green-$\mathcal{M}_3$ and red-$\mathcal{M}_4$.

−30 and 0/10 °C, while at higher temperatures the variations are more limited.

Fig. 16 illustrates the relative variation of each parameter with reference to its value at the room temperature of 20 °C. The relative variation is presented for the parameters of MSFRC1 (Fig. 16(a)), MSFRC2 (Fig. 16(b)) and MSFRC3 (Fig. 16(c)). First, the focus is on the parameters that mainly influence the flexural response, namely f_{ct}, $g(w_1)$ and $g(w_2)$. f_{ct} has a decreasing trend with a maximum variation at −30 °C of 84% for MSFRC1, 116% for MSFRC2 and 136% for MSFRC3. The highest negative variation is reached at 60 °C and is −24% (MSFRC1), −31% (MSFRC2) and −25% (MSFRC3). The maximum positive variation of $g(w_1)$ and $g(w_2)$ is obtained at the transition temperature, which is approximately −1.5 °C for MSFRC1 and 10 °C for MSFRC2 and MSFRC3. Two decreasing trends are observed for temperature changes below and above the transition temperature. The sensitivity to the temperature change below the transition temperature is larger for MSFRC1 and MSFRC3. Considering in the order $g(w_1)$ and $g(w_2)$, the highest negative variation for these parameters is [−42%, −31%] for MSFRC1, [−38%, −51%] for MSFRC2 and [−45%, −41%] for MSFRC3. As concerns the remaining parameters, w_1 and w_2 are generally more sensitive to the temperature change above the transition

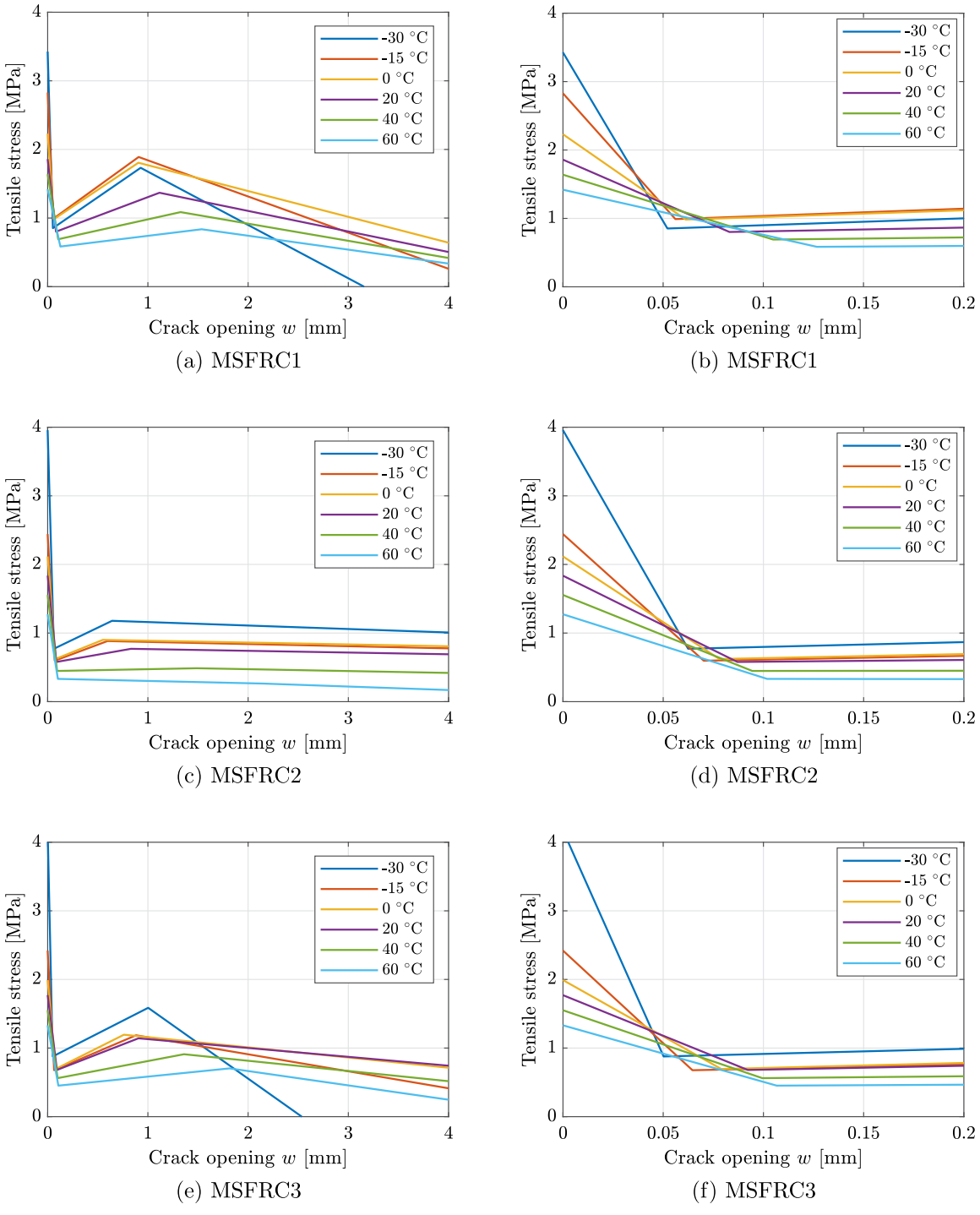

Fig. 15. Variation of the trilinear constitutive relationship with temperature predicted by model $\mathcal{M}_3$ for (a, b) MSFRC1, (c, d) MSFRC2 and (e, f) MSFRC3.

Table 4
Estimated coefficients of the analyzed regression models for MSFRC3.

Par.	Coef.	Unit	$\mathcal{M}_1$	$\mathcal{M}_2$	$\mathcal{M}_3$	$\mathcal{M}_4$
f_{ct}	$\beta_{1,1}$	[MPa]	2.47	$7.24{\cdot}10^{-1}$	$6.68{\cdot}10^{-1}$	$3.41{\cdot}10^{-1}$
	$\beta_{1,2}$	[MPa·°C^{-1}]	$-2.10{\cdot}10^{-2}$	$-1.14{\cdot}10^{-1}$	$-1.17{\cdot}10^{-1}$	$-1.28{\cdot}10^{-1}$
	$\beta_{1,3}$	[MPa·°C^{-1}]	–	$-1.17{\cdot}10^{-2}$	$-1.10{\cdot}10^{-2}$	$-1.28{\cdot}10^{-2}$
	$\beta_{1,4}$	[°C]	–	−12.6	−12.5	−15.0
w_1	$\beta_{2,1}$	[mm]	$6.93{\cdot}10^{-2}$	$7.30{\cdot}10^{-2}$	$7.90{\cdot}10^{-2}$	$8.97{\cdot}10^{-2}$
	$\beta_{2,2}$	[mm·°C^{-1}]	$6.11{\cdot}10^{-7}$	$7.31{\cdot}10^{-4}$	$9.60{\cdot}10^{-4}$	$1.34{\cdot}10^{-3}$
	$\beta_{2,3}$	[mm·°C^{-1}]	–	$7.57{\cdot}10^{-4}$	$3.60{\cdot}10^{-4}$	$5.46{\cdot}10^{-4}$
	$\beta_{2,4}$	[°C]	–	39.5	10.1	−15.0
$g(w_1)$	$\beta_{3,1}$	[-]	$2.97{\cdot}10^{-1}$	$3.49{\cdot}10^{-1}$	$3.49{\cdot}10^{-1}$	$4.75{\cdot}10^{-1}$
	$\beta_{3,2}$	[°C^{-1}]	$1.48{\cdot}10^{-3}$	$4.58{\cdot}10^{-3}$	$4.62{\cdot}10^{-3}$	$8.93{\cdot}10^{-3}$
	$\beta_{3,3}$	[°C^{-1}]	–	$-1.46{\cdot}10^{-3}$	$-1.11{\cdot}10^{-3}$	$-9.38{\cdot}10^{-6}$
	$\beta_{3,4}$	[°C]	–	11.9	10.1	−15.0
Δw_{1-2}	$\beta_{4,1}$	[mm]	1.03	$7.61{\cdot}10^{-1}$	$6.82{\cdot}10^{-1}$	$9.01{\cdot}10^{-1}$
	$\beta_{4,2}$	[mm·°C^{-1}]	$7.37{\cdot}10^{-3}$	$-6.64{\cdot}10^{-3}$	$-9.03{\cdot}10^{-3}$	$-6.16{\cdot}10^{-4}$
	$\beta_{4,3}$	[mm·°C^{-1}]	–	$2.11{\cdot}10^{-2}$	$2.24{\cdot}10^{-2}$	$4.25{\cdot}10^{-5}$
	$\beta_{4,4}$	[°C]	–	13.4	10.1	−15.0
$g(w_2)$	$\beta_{5,1}$	[-]	$5.18{\cdot}10^{-1}$	$6.04{\cdot}10^{-1}$	$6.00{\cdot}10^{-1}$	$7.61{\cdot}10^{-1}$
	$\beta_{5,2}$	[°C^{-1}]	$1.14{\cdot}10^{-3}$	$7.37{\cdot}10^{-3}$	$7.33{\cdot}10^{-3}$	$1.28{\cdot}10^{-2}$
	$\beta_{5,3}$	[°C^{-1}]	–	$-2.41{\cdot}10^{-3}$	$-2.91{\cdot}10^{-3}$	$-1.73{\cdot}10^{-5}$
	$\beta_{5,4}$	[°C]	–	8.1	10.1	−15.0
$g(\bar{w})$	$\beta_{6,1}$	[-]	$2.32{\cdot}10^{-1}$	$5.16{\cdot}10^{-1}$	$5.53{\cdot}10^{-1}$	$8.97{\cdot}10^{-1}$
	$\beta_{6,2}$	[°C^{-1}]	$5.90{\cdot}10^{-3}$	$1.89{\cdot}10^{-2}$	$1.99{\cdot}10^{-2}$	$3.07{\cdot}10^{-2}$
	$\beta_{6,3}$	[°C^{-1}]	–	$-8.37{\cdot}10^{-3}$	$-1.09{\cdot}10^{-2}$	$-1.45{\cdot}10^{-5}$
	$\beta_{6,4}$	[°C]	–	10.5	10.1	−15.0

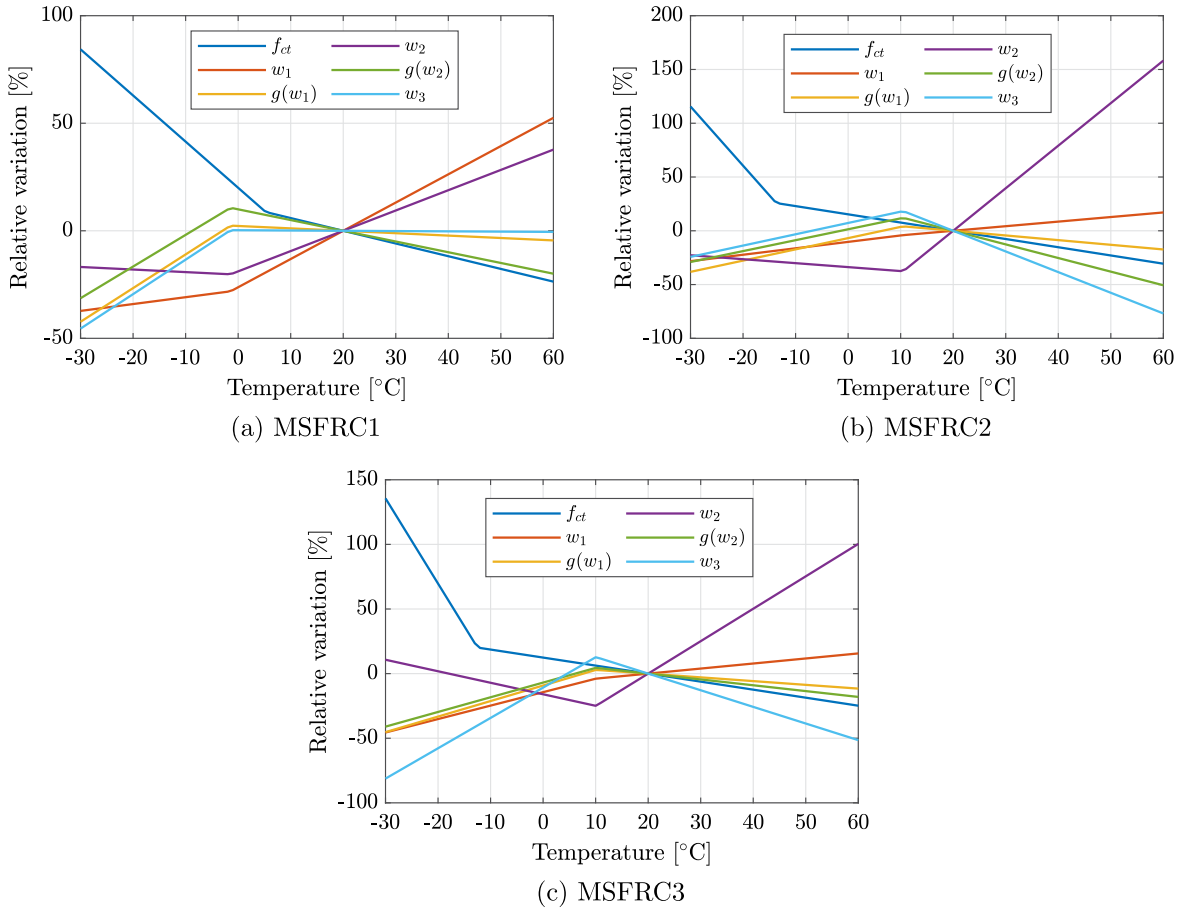

Fig. 16. Relative variation of the constitutive parameters with respect to their value at the room temperature predicted by model $\mathcal{M}_3$ for (a) MSFRC1, (b) MSFRC2 and (c) MSFRC3.

temperature. The variation of w_3 with temperature exhibits a trend similar to that of $g(w_1)$ and $g(w_2)$. The flexural response of the model is not very sensitive to the variation of w_1, w_2 and w_3 within ranges of engineering interest, hence further details are not indicated.

Table 5
Performance of the competing models. Minimum values in bold.

	J_{gl}				AIC_C			
	$\mathcal{M}_1$	$\mathcal{M}_2$	$\mathcal{M}_3$	$\mathcal{M}_4$	$\mathcal{M}_1$	$\mathcal{M}_2$	$\mathcal{M}_3$	$\mathcal{M}_4$
MSFRC1	152.0	**110.9**	111.2	111.6	2453.9	2441.0	2430.1	**2427.9**
MSFRC2	127.5	**83.2**	83.5	88.0	2429.0	2400.3	**2389.5**	2394.1
MSFRC3	134.0	**77.9**	77.9	88.7	2436.1	2390.9	**2379.5**	2395.3

6. Conclusions

This paper investigates the temperature effect on the flexural behavior of polypropylene macro-synthetic fiber reinforced concrete. First, an extensive experimental campaign is carried out on specimens with different properties conserved at different temperatures, namely −30 °C, −15 °C, 0 °C, 20 °C, 40 °C and 60 °C. The analysis of experimental results shows the influence of temperature on compression and flexural tensile strengths. An additional study is then realized for estimating the dependency between the parameters of a tensile constitutive relationship and temperature. The parameters are obtained by means of inverse analysis of a cracked hinge model.

An hybrid regression model is developed to describe this dependency. Moreover, the most adequate regression model is selected among several alternatives according to the Akaike Information Criterion. The selected model involves a dependency of bi-linear type for each parameter. Only two transition temperatures are required, one for the tensile strength and the other for the remaining parameters of the constitutive relationship. This model proves to be well suited to describe the temperature effect for different polypropylene macro-synthetic fiber reinforced concretes.

The predicted variations of the constitutive parameters with temperature ranging in the interval [−30 60] ° C are remarkable. For example, the maximum relative variation of the tensile strength with reference to the value at the room temperature is of the order of 80% - 130%. Even the relative variation of the other parameters is significant and it ranges from 20% to 80%.

The results of this work can be employed for prediction purposes with specific reference to the adopted materials. Finally, the presented procedure and the selected regression model can be taken as a reference for modeling the temperature effect on fiber reinforced concretes constituted by materials of different properties.

CRediT authorship contribution statement

Federico Ponsi: Writing – review & editing, Writing – original draft, Validation, Software, Methodology, Data curation, Conceptualization. **Elisa Bassoli:** Writing – review & editing, Writing – original draft, Methodology, Data curation, Conceptualization. **Claudio Mazzotti:** Writing – review & editing, Writing – original draft, Validation, Supervision, Methodology, Conceptualization. **Nicola Buratti:** Writing – review & editing, Writing – original draft, Validation, Supervision, Methodology, Conceptualization. **Loris Vincenzi:** Writing – review & editing, Writing – original draft, Validation, Supervision, Software, Methodology, Data curation, Conceptualization.

Declaration of competing interest

The authors declare that they have no known competing financial interests or personal relationships that could have appeared to influence the work reported in this paper.

Acknowledgments

The numerical studies presented in this paper were sponsored by the Department of Engineering “Enzo Ferrari” of the University of Modena and Reggio Emilia (Italy) via the research project “Modellazione probabilistica del comportamento meccanico di calcestruzzi fibrorinforzati al variare della temperatura” in the scope of the research grant FARD-2024-2025. The financial support of the University of Modena and Reggio Emilia is gratefully acknowledged.

Data availability

Data will be made available on request.

References

[1] F. Ortiz Navas, J. Navarro-Gregori, G. Leiva Herdocia, P. Serna, E. Cuenca, An experimental study on the shear behaviour of reinforced concrete beams with macro-synthetic fibres, Constr. Build. Mater. 169 (2018) 888–899, http://dx.doi.org/10.1016/j.conbuildmat.2018.02.023, URL https://www.sciencedirect.com/science/article/pii/S0950061818302484.

[2] V. Dey, A. Bonakdar, B. Mobasher, Low-velocity flexural impact response of fiber-reinforced aerated concrete, Cem. Concr. Compos. 49 (2014) 100–110, http://dx.doi.org/10.1016/j.cemconcomp.2013.12.006, URL https://www.sciencedirect.com/science/article/pii/S0958946513002059.

[3] A.M. Brandt, Fibre reinforced cement-based (FRC) composites after over 40 years of development in building and civil engineering, Compos. Struct. 86 (1–3) (2008) 3–9.

[4] M. di Prisco, FRC: structural applications and standards, Mater. Struct. 42 (9) (2009) 1169–1171.

[5] N. Yermak, P. Pliya, A.-L. Beaucour, A. Simon, A. Noumowé, Influence of steel and/or polypropylene fibres on the behaviour of concrete at high temperature: Spalling, transfer and mechanical properties, Constr. Build. Mater. 132 (2017) 240–250, http://dx.doi.org/10.1016/j.conbuildmat.2016.11.120, URL https://www.sciencedirect.com/science/article/pii/S095006181631889X.

[6] Y.-s. Kim, T.-g. Lee, G.-y. Kim, An experimental study on the residual mechanical properties of fiber reinforced concrete with high temperature and load, Mater. Struct. 46 (4) (2013) 607–620.

[7] H. Wu, X. Lin, A. Zhou, A review of mechanical properties of fibre reinforced concrete at elevated temperatures, Cem. Concr. Res. 135 (2020) 106117, http://dx.doi.org/10.1016/j.cemconres.2020.106117, URL https://www.sciencedirect.com/science/article/pii/S0008884619314267.

[8] N. Buratti, C. Mazzotti, Experimental tests on the effect of temperature on the long-term behaviour of macrosynthetic fibre reinforced concretes, Constr. Build. Mater. 95 (2015) 133–142, http://dx.doi.org/10.1016/j.conbuildmat.2015.07.073, URL https://www.sciencedirect.com/science/article/pii/S0950061815301045.

[9] M. Caballero-Jorna, M. Roig Flores, P. Serna, A study of the flexural behavior of fiber-reinforced concretes exposed to moderate temperatures, Materials 14 (2021) 3522, http://dx.doi.org/10.3390/ma14133522.

[10] S. Aidarov, A. Nogales, I. Reynvart, N. Tošić, A. de la Fuente, Effects of low temperatures on flexural strength of macro-synthetic fiber reinforced concrete: Experimental and numerical investigation, Materials 15 (3) (2022) http://dx.doi.org/10.3390/ma15031153, URL https://www.mdpi.com/1996-1944/15/3/1153.

[11] A. Richardson, R. Ovington, Temperature related steel and synthetic fibre concrete performance, Constr. Build. Mater. 153 (2017) 616–621, http://dx.doi.org/10.1016/j.conbuildmat.2017.07.101, URL https://www.sciencedirect.com/science/article/pii/S0950061817314332.

[12] J. Zhengwu, D. Zilong, Z. Xinping, L. Wenting, Increased strength and related mechanisms for mortars at cryogenic temperatures, Cryogenics 94 (2018) 5–13, http://dx.doi.org/10.1016/j.cryogenics.2018.06.005, URL https://www.sciencedirect.com/science/article/pii/S0011227518301140.

[13] H. Lin, Y. Han, S. Liang, F. Gong, S. Han, C. Shi, P. Feng, Effects of low temperatures and cryogenic freeze-thaw cycles on concrete mechanical properties: A literature review, Constr. Build. Mater. 345 (2022) 128287, http://dx.doi.org/10.1016/j.conbuildmat.2022.128287, URL https://www.sciencedirect.com/science/article/pii/S0950061822019481.

[14] U. Schneider, U. Diederichs, C. Ehm, Effect of temperature on steel and concrete for PCRV's, Nucl. Eng. Des. 67 (2) (1982) 245–258, http://dx.doi.org/10.1016/0029-5493(82)90144-3, URL https://www.sciencedirect.com/science/article/pii/0029549382901443.

[15] G. Srikar, G. Anand, S. Suriya Prakash, A study on residual compression behavior of structural fiber reinforced concrete exposed to moderate temperature using digital image correlation, Int. J. Concr. Struct. Mater. 10 (1) (2016) 75–85.

[16] A. Gibson, M.O. Torres, T. Browne, S. Feih, A. Mouritz, High temperature and fire behaviour of continuous glass fibre/polypropylene laminates, Compos. Part A: Appl. Sci. Manuf. 41 (9) (2010) 1219–1231, http://dx.doi.org/10.1016/j.compositesa.2010.05.004, Special Issue on 10th Deformation & Fracture of Composites Conference: Interfacial interactions in composites and other applications. URL https://www.sciencedirect.com/science/article/pii/S1359835X10001338.

[17] A. Bentur, S. Mindess, et al., Fibre Reinforced Cementitious Composites, Crc Press, 2006.
[18] M. Tanaka, G.S. Dulikravich, Inverse Problems in Engineering Mechanics, Elsevier, 1998.
[19] A. Nour, B. Massicotte, R. de Montaignac, J.-P. Charron, Development of an inverse analysis procedure for the characterisation of softening diagrams for FRC beams and panels, Constr. Build. Mater. 94 (2015) 35–44, http://dx.doi.org/10.1016/j.conbuildmat.2015.06.049, URL https://www.sciencedirect.com/science/article/pii/S0950061815300064.
[20] L. Vincenzi, F. Ponsi, E. Bassoli, N. Buratti, A computationally efficient procedure for calibrating model parameters of multiple specimens, Constr. Build. Mater. 411 (2024) 134757, http://dx.doi.org/10.1016/j.conbuildmat.2023.134757, URL https://www.sciencedirect.com/science/article/pii/S0950061823044781.
[21] F. Ponsi, E. Bassoli, N. Buratti, L. Vincenzi, Parameter estimation and uncertainty quantification of a fiber-reinforced concrete model by means of a multi-level Bayesian approach, Constr. Build. Mater. 438 (2024) 136994, http://dx.doi.org/10.1016/j.conbuildmat.2024.136994, URL https://www.sciencedirect.com/science/article/pii/S0950061824021366.
[22] S. Mishra, R. Wan-Wendner, C.D. Prete, C. Mazzotti, N. Buratti, Numerical study on the behavior of polypropylene fiber reinforced concrete subjected to moderate temperature variations using LDPM theory, Constr. Build. Mater. 417 (2024) 135424, http://dx.doi.org/10.1016/j.conbuildmat.2024.135424, URL https://www.sciencedirect.com/science/article/pii/S0950061824005658.
[23] H. Akaike, A new look at the statistical model identification, IEEE Trans. Autom. Control 19 (6) (1974) 716–723, http://dx.doi.org/10.1109/TAC.1974.1100705.
[24] EN 14651:2005+A1:2007 - Test method for metallic fibre concrete – Measuring the flexural tensile strength (limit of proportionality (LOP), residual), 2007, European Committee for Standardization (CEN), Brussels: CEN. Standard + Amendment A1.
[25] Eurocode 1: Actions on structures - part 1-5: General actions - thermal actions, 2003.
[26] J. Brandrup, E.H. Immergut, E.A. Grulke, A. Abe, D.R. Bloch, Polymer Handbook, fourth ed., John Wiley & Sons, 2005.
[27] L. Jin, B. Lu, W. Yu, C. Xie, X. Du, Direct tensile failures of concrete with various moisture contents and sizes at low temperatures via mesoscale simulations with ice explicit modelling, Constr. Build. Mater. 449 (2024) 138300, http://dx.doi.org/10.1016/j.conbuildmat.2024.138300, URL https://www.sciencedirect.com/science/article/pii/S0950061824034421.
[28] Y. Wang, Z. Wu, X. Zheng, K. Li, C. Liu, A review of concrete exposed to low-temperature environments at early ages: mechanical properties and durability, J. Build. Eng. 111 (2025) 113122, http://dx.doi.org/10.1016/j.jobe.2025.113122, URL https://www.sciencedirect.com/science/article/pii/S2352710225013592.
[29] W. Zhao, Z. Dawei, G. Fuyuan, M. Saeid, U. Tamon, Multiscale modeling and simulation of ice-strengthening effects in mesocracks of saturated frost-damaged concrete under freezing temperature, J. Mater. Civ. Eng. 33 (2) (2025) 04020443, http://dx.doi.org/10.1061/(asce)mt.1943-5533.0003450.
[30] N. Buratti, C. Mazzotti, M. Savoia, Post-cracking behaviour of steel and macro-synthetic fibre-reinforced concretes, Constr. Build. Mater. 25 (5) (2011) 2713–2722.
[31] C. Del Prete, N. Buratti, C. Mazzotti, Experimental investigation on the influence of temperature variations on macro-synthetic fibre reinforced concrete short and long term behaviour, in: P. Serna, A. Llano-Torre, J.R. Martí Vargas, J. Navarro-Gregori (Eds.), Fibre Reinforced Concrete: Improvements and Innovations II, Springer International Publishing, Cham, 2022, pp. 331–341.
[32] M. Jarrigeon, B. Chabert, D. Chatain, C. Lacabanne, G. Nemoz, Multiple transitions in isotactic polypropylene around and above the glass transition, J. Macromol. Sci. Part B 17 (1) (1980) 1–24, http://dx.doi.org/10.1080/00222348008212795.
[33] J. Olesen, Fictitious crack propagation in fiber-reinforced concrete beams, J. Eng. Mech. 127 (3) (2001) 272–280.
[34] J.P. Ulfkjær, S. Krenk, R. Brincker, Analytical modelfor fictitious crack propagation in concrete beams, J. Eng. Mech. ASCE 121 (1) (1995) 7–15, http://dx.doi.org/10.1061/(ASCE)0733-9399(1995)121:1(7).
[35] K. Chiranjeevi Reddy, K.V. Subramaniam, Analysis for multi-linear stress-crack opening cohesive relationship: Application to macro-synthetic fiber reinforced concrete, Eng. Fract. Mech. 169 (2017) 128–145, http://dx.doi.org/10.1016/j.engfracmech.2016.11.015.
[36] S.J. Stephen, B. Raphael, R. Gettu, S. Jose, Determination of the tensile constitutive relations of fiber reinforced concrete using inverse analysis, Constr. Build. Mater. 195 (2019) 405–414, http://dx.doi.org/10.1016/j.conbuildmat.2018.11.014, URL https://www.sciencedirect.com/science/article/pii/S0950061818326795.
[37] S. Gali, K.V. Subramaniam, Multi-linear stress-crack separation relationship for steel fiber reinforced concrete: Analytical framework and experimental evaluation, Theor. Appl. Fract. Mech. 93 (2018) 33–43, http://dx.doi.org/10.1016/j.tafmec.2017.06.018, URL https://www.sciencedirect.com/science/article/pii/S0167844217300952.
[38] J. Sous, R. Gettu, Determining the tensile stress-crack opening curve of concrete by inverse analysis, J. Eng. Mech. 132 (2) (2006) 141–148, http://dx.doi.org/10.1061/(ASCE)0733-9399(2006)132:2(141).
[39] L. Vincenzi, P. Gambarelli, A proper infill sampling strategy for improving the speed performance of a surrogate-assisted evolutionary algorithm, Comput. Struct. 178 (2017) 58–70, http://dx.doi.org/10.1016/j.compstruc.2016.10.004.
[40] F. Ponsi, E. Bassoli, N. Buratti, L. Vincenzi, Development of a hybrid regression model for predicting the mechanical behavior of macrosynthetic fiber reinforce concrete, Constr. Build. Mater. 483 (2025) 141582, http://dx.doi.org/10.1016/j.conbuildmat.2025.141582, URL https://www.sciencedirect.com/science/article/pii/S0950061825017325.
[41] S. Kullback, R.A. Leibler, On information and sufficiency, Ann. Math. Stat. 22 (1951) 79–86, URL https://api.semanticscholar.org/CorpusID:120349231.
[42] C.M. Hurvich, C.-L. Tsai, Regression and time series model selection in small samples, Biometrika 76 (2) (1989) 297–307, http://dx.doi.org/10.1093/biomet/76.2.297, arXiv:https://academic.oup.com/biomet/article-pdf/76/2/297/737009/76-2-297.pdf.
[43] L. Ljung, System identification: Theory for the user, in: Prentice Hall information and system sciences series, Prentice Hall PTR, 1999, URL https://books.google.it/books?id=nHFoQgAACAAJ.
[44] J. Guo, S. Mu, C. Yu, C. Hu, F. Guan, H. Zhang, Y. Gong, Mechanical and thermal properties of polypropylene/modified basalt fabric composites, J. Appl. Polym. Sci. 132 (36) (2025).